

January 26, 2005

MSU-HEP-5  
CTEQ-5

# Stability of NLO Global Analysis and Implications for Hadron Collider Physics

J. Huston, J. Pumplin, D. Stump, W.K. Tung

Michigan State University, E. Lansing, MI 48824

# Contents

<b>1</b>	<b>Introduction</b>	<b>2</b>
<b>2</b>	<b>Issues related to the stability of NLO global analysis</b>	<b>3</b>
<b>3</b>	<b>Inputs to the current analysis</b>	<b>7</b>
<b>4</b>	<b>Results on the stability of NLO global analysis</b>	<b>7</b>
4.1	Stability with respect to kinematic cuts on input data . . . . .	8
4.2	Stability and $\alpha_s$ . . . . .	10
4.3	Comments and Discussions . . . . .	12
<b>5</b>	<b>Stability and Uncertainty of <math>\sigma_W^{\text{tot}}</math> at the LHC</b>	<b>13</b>
<b>6</b>	<b>Conclusions</b>	<b>15</b>
<b>A</b>	<b>Treatment of <math>\alpha_s(Q)</math></b>	<b>16</b>
<b>B</b>	<b>PDFs at small <math>x</math>: do they go negative?</b>	<b>17</b>
<b>C</b>	<b>Gluon distribution at large <math>x</math>: do counting rules count?</b>	<b>19</b>

# 1 Introduction

A critical element of progress in high energy physics research is the continued improvement of global QCD analysis of parton distribution functions (PDFs), which link measured hadronic cross sections to the underlying partonic processes of the fundamental theory. Precision tests of the Standard Model and searches for New Physics in the next generation of collider programs at the Tevatron and the LHC will depend on accurate PDFs and reliable estimates of the PDF uncertainties.

The vast majority of work on global QCD analysis of PDFs and the application of these distributions to the calculation of high energy processes has been performed at the next-to-leading order (NLO) approximation of perturbation theory, i.e., 1-loop hard cross sections and 2-loop evolution kernels. For NLO calculations in QCD, the order of magnitude of the neglected remainder terms in the perturbative expansion is  $\sim \alpha_s^2$  with respect to the leading terms. Thus, the theoretical uncertainty of the predicted cross sections at the energy scales of colliders should be less than a few percent. This level of accuracy is adequate for current phenomenology, since experimental errors are either comparable in size (for high-precision deep inelastic scattering (DIS) measurements) or larger (for most other processes).<sup>1</sup>

In recent years, some preliminary next-to-next-leading-order (NNLO) analyses have been carried out either for DIS alone [1], or in a global analysis context [2] (even if the necessary hard cross sections for some processes, such as inclusive jet production, are not yet available at this order).<sup>2</sup> The differences with respect to the corresponding NLO analyses were indeed of the expected order of magnitude, including regions close to kinematic boundaries where the differences are somewhat larger than that due to power-counting of  $\alpha_s$  alone. The NNLO calculations are considerably more complex than the NLO ones. Application of these results in global analyses or experimental simulations can be computationally costly or even impractical. However, NLO analyses are perfectly adequate as long as their estimated accuracy is sufficient for the task, and as long as the predictions are stable with respect to certain choices inherent to the analysis. Two examples of the latter are the functional forms used to parametrize the initial non-perturbative parton distribution functions, and the selection of experimental data sets used in the fit, including kinematic cuts imposed on the data points in the selected sets.

In global QCD analyses, kinematic cuts on the variables  $x$ ,  $Q$ ,  $W$ ,  $p_t$ , etc. are made in order to suppress higher order contributions, unaccounted edge-of-phase-space effects, power-law corrections, small- $x$  evolution effects, and other non-perturbative theoretical effects. In the absence of a complete understanding of these effects, the optimal choices for the cuts must

---

<sup>1</sup>Exceptions include: (i) specific processes for which the perturbative expansion is known to converge more slowly (e.g. direct photon production); and (ii) processes near kinematic boundaries, where resummation of certain large logarithms becomes necessary (e.g. small- $x$  in DIS). These exceptional circumstances have not become phenomenologically significant in global QCD analysis so far.

<sup>2</sup>The NNLO evolution kernel was also only known approximately at the time of these analyses. This gap has now been closed [3].

be determined empirically. We must compare results of global analyses done with various kinematic cuts on the data, and find regions of stability (internal consistency) at LO, NLO, or NNLO. From studies of this kind, NLO CTEQ analyses have used the following set of “standard cuts” for DIS data:  $Q > 2 \text{ GeV}$  and  $W > 3.5 \text{ GeV}$ . The standard MRST analyses use cuts of  $Q > 1.41 \text{ GeV}$  and  $W > 3.54 \text{ GeV}$ .

The stability of NLO global analyses has, however, been seriously challenged by recent MRST analyses [4], which found a 20% variation in the cross section predicted for W production at the LHC—a very important “standard candle” process for hadron colliders—when certain cuts on input data are varied. If this instability is verified, it would significantly impact the phenomenology of a wide range of physical processes for the Tevatron Run II and the LHC. We have therefore performed an independent study of this issue within the framework of the CTEQ global analysis. In addition, to explore the dependence of the results on assumptions made about the parametrization of PDFs at our starting scale  $Q_0 = 1.3 \text{ GeV}$ , we also studied the effect of allowing a negative gluon PDF at small  $x$ —a possibility favored by the MRST NLO analysis which appears to be tied to the stability issue.

In Sec. 2 we discuss issues relevant to the stability problem. In Sec. 3 we summarize the theoretical and experimental inputs to the global analyses. In Sec. 4, we describe the detailed results of our study. The main conclusion is that we find both the NLO PDFs and their physical predictions at the Tevatron and the LHC to be quite stable with respect to variations of the kinematic cuts and the parametrization. Since this conclusion is quite different from those of the MRST study, potential sources of the difference are discussed. In Sec. 5, predictions on the total cross section of W production and their uncertainties are studied in more detail using the robust Lagrangian multiplier method, with particular attention to the stability issue. The Appendix contains more detailed discussions on three issues that come up in the comparison of CTEQ and MRST analyses described in Sections 4 and 5: (i) the definition of  $\alpha_s$ ; (ii) small- $x$  behavior of PDFs and negative  $g(x, Q)$ ; and (iii) large- $x$  behavior of  $g(x, Q)$  and quark counting rules.

In addition to the CTEQ and MRST global analyses, there are other global analysis efforts, which focus mainly on DIS data [5–8]. However, they do not address the stability issue (because it is the interplay between DIS, DY and Jet data sets that raises the issue). For this reason, our discussions will consider only results from the two global analysis groups that include all three types of hard processes.

## 2 Issues related to the stability of NLO global analysis

There are three issues in the global analysis of PDFs that may affect the stability with respect to kinematic cuts on the input data: HERA data at low  $x$ , Tevatron jet data, and the parametrization of the gluon distribution  $g(x)$ . In this section, we provide some background on these issues, before describing our independent study of the stability of NLO global analysis in later sections.

The main evidence for instability of the NLO global analyses observed in Ref. [4] is shown in Fig. 1. Plot (a) shows the variation of the predicted total cross section for  $W$  production at the LHC, as a function of the kinematic cut on the Bjorken variable  $x$  in DIS. For the largest  $x$  cut ( $=0.01$ ) the NLO prediction is 20% lower than the standard prediction; they are clearly incompatible. Plot (b) shows the predicted rapidity distribution

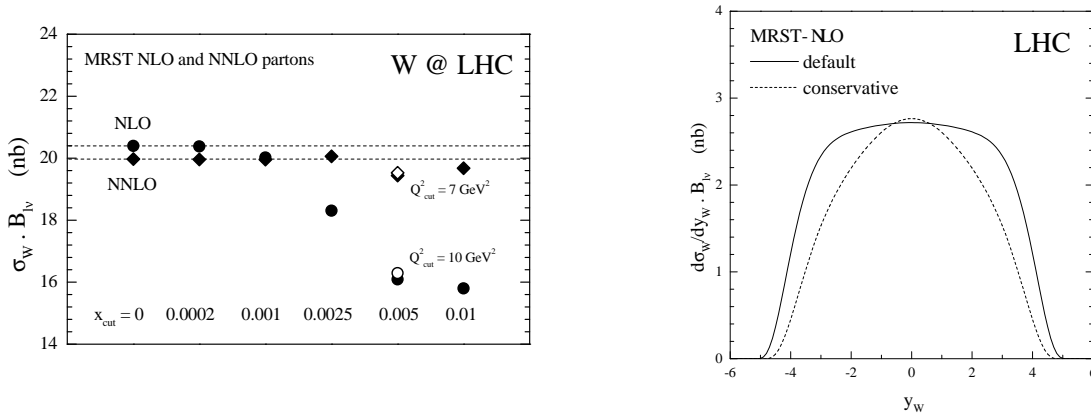


Figure 1: (a) Dependence of the MRST predictions for the total  $W$  production cross section at the LHC on kinematic cuts on input data used in the global analysis; (b) the  $W$  rapidity distribution according to the MRST default PDFs, and the “conservative” PDFs (based on relatively high  $x$  and  $Q$  cuts). Both figures are reproduced from [4].

of the produced  $W$  boson for the “conservative fit” (the one with the largest  $x$ -cut); the distribution drops steeply compared to that of the standard fit outside the central rapidity region, thus producing the drop in  $\sigma_W$  seen in plot (a). This effect was attributed to a *tension* between the Tevatron inclusive jet data and the DIS data at small  $x$  (HERA) and medium  $x$  (NMC), cf. Ref. [4]. That tension is gradually relaxed as the  $x$ -cut is raised, i.e., as more small- $x$  data are excluded. Evidently, removing the HERA constraint, and thus effectively placing more emphasis on the inclusive jet data, significantly changes the PDFs and the resulting prediction of  $\sigma_W^{LHC}$ . In the MRST global analysis, the combined data also pull the gluon distribution to negative values at small  $x$  and small  $Q$ . It is likely that these two problems—the instability of the prediction on  $\sigma_W$  and the negative gluon PDF—are interrelated.

The CTEQ and MRST global analyses use much of the same data sets, theory input and analysis methods. Hence they usually yield results that are in general agreement. However, minor differences between the choices that are made for these inputs can, under some circumstances, give rise to discernible differences in the resulting PDFs and their predictions. For example, in Fig. 2a the fractional uncertainty of the  $u$ -quark distribution at  $Q^2 = 10 \text{ GeV}^2$ , normalized to CTEQ6.1M [9], is shown as the shaded band for  $10^{-4} < x < 0.9$ . The comparison curves are CTEQ6M [10] (dotted black), MRST2002 [11] (solid blue) and

MRST2003c [4] (dashed red) and the reference CTEQ6.1M (solid horizontal).<sup>3</sup> We see that: (i) the uncertainty is small,  $\sim 5\%$  for much of the  $x$ -range; and (ii) with the exception of MRST2003c (“c” for *conservative*) at small  $x$ , the other standard fits agree reasonably well. This reflects the tight constraints imposed by the precise DIS and DY data.

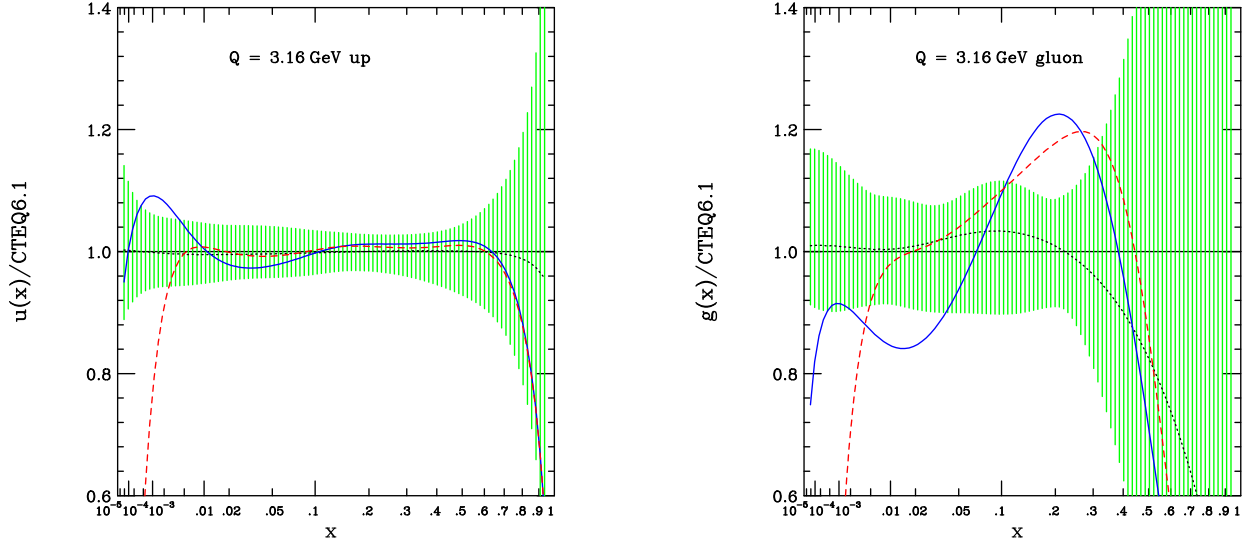


Figure 2: Comparison of the CTEQ6.1M and MRST2002 PDFs, for (a) the u-quark and (b) the gluon distributions at  $Q^2 = 10 \text{ GeV}^2$ . The scale of the  $x$ -axis, as indicated, is chosen to exhibit both the large- $x$  and the small- $x$  regions clearly. The vertical axis is the ratio of the specified PDF set to CTEQ6.1M. (Dotted (Black) = CTEQ6; Solid (Blue) = mrst2002; Dashed (Red) = mrst2003c.)

The corresponding comparison for the gluon distribution, is shown in Fig. 2b. We see that the fractional uncertainty is much larger in this case, especially for  $x > 0.25$ . Even taking into account the size of the uncertainties, the difference in shape between the MRST and CTEQ gluon distributions over the full range of  $x$  is evident. The differences between the MRST and CTEQ standard fits are indicative of how the small-to-medium  $x$  DIS data and the medium-to-large  $x$  Tevatron inclusive jet data are being fit differently in the two analyses (to be discussed below). Also noticeable is the change in shape of  $g(x, Q)$  below  $x \sim 0.1$  between the default and conservative MRST distributions. This difference shows the effect of removing DIS data at small  $x$ .

The gluon distribution is related rather directly to the jet data. The larger gluon at high  $x$  in the CTEQ6.1M PDF set leads to a larger predicted cross section at high jet  $E_T$ , in better agreement with the Tevatron data. Quantitatively, the  $\chi^2$  for the Tevatron Run 1 CDF and D0 jet is 118 for 123 data points in the CTEQ6.1M fit. The corresponding numbers for recent standard MRST fits are  $\sim 160$  for 115 data points [4, 11]. Fig. 3 shows 4  $\eta$  bins of

<sup>3</sup>The choice of the  $x$ -scale, specified in the figure caption, exhibits details from both small  $x$  and large  $x$  on one graph.

the D0 data, along with the theoretical curves obtained with CTEQ6.1M, MRST2002 and MRST2003c PDFs.<sup>4</sup> In the PDF parametrization adopted in the standard MRST fits, the

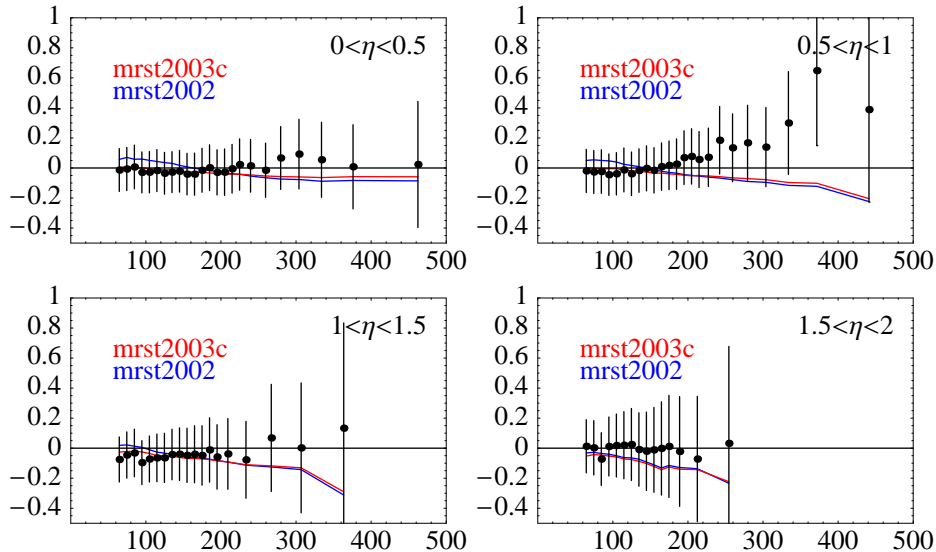


Figure 3: Comparison between the D0 jet data and cross sections calculated with CTEQ6.1M, MRST2002, and MRST2002-conservative PDFs.

rather high value of  $\chi^2$  for the jet cross section is caused by a trade-off with the  $\chi^2$  of DIS data at small-to-medium  $x$  (hence the *tension*) [4, 11]. This tension is relaxed only when DIS data with  $x < 0.005$ , and  $Q^2 < 10 \text{ GeV}^2$  are removed from the fit, resulting in the conservative fit (mrst2003c). This reduced the  $\chi^2$  for the jet data sets significantly [4, 12]. The reduction in  $\chi^2$  occurs mostly in the low transverse momentum range (100-200 GeV/c) for low rapidities, where the errors are relatively small—a fact not immediately springing out of the paper in a casual glance of Fig. 3.

The significant differences between the MRST standard and conservative fits, and their physical predictions (cf. Fig. 1) highlight the instability of these NLO QCD global analyses. The "conservative" fit, although free from apparent tension, cannot be considered as a serious candidate for calculating safer physical predictions [4].<sup>5</sup> First, the removal of the high precision small- $x$  and low- $Q$  DIS data results in the loss of powerful constraints on the PDFs, especially for small- $x$ . This gives rise generally to much increased uncertainties in physical predictions that depend on small- $x$  PDFs—i.e. much of collider physics at LHC and beyond. Furthermore, in the particular case of mrst2003c, the gluon distribution becomes strongly negative at small  $x$  as seen in Figs. .... This leads to negative predictions for physical quantities (such as  $F_L$  in DIS and  $d\sigma_W/dy$  at large  $y$  and very high energies).

<sup>4</sup>The D0 data separated in  $\eta$  bins are more sensitive to the behavior of the gluon distribution over a wider range of  $x$  than the CDF data which is limited to central rapidity. The highest  $\eta$  bin measured by D0 is not shown here since they are not included in the MRST analyses.

<sup>5</sup>Robert Thorne, private communications.

In the MRST analyses, stability of the global fits is restored only at NNLO. On the other hand, all existing CTEQ NLO global analyses have not shown any signs of tension between the inclusive jet data and the DIS data. Therefore it is important to investigate the stability issue in more detail within the CTEQ framework to see whether QCD analysis of collider physics phenomenology is viable at NLO in general, as usually expected.

### 3 Inputs to the current analysis

The new global analyses are extensions of the CTEQ6 analysis. We briefly summarize the theoretical and experimental inputs in this section. Some of these features are relevant for later discussions on the comparison of our results with those of Ref. [4]. For details, see the CTEQ6 paper [10].

We use the  $\overline{\text{MS}}$  scheme in the conventional PQCD framework, with three light quark flavors ( $u, d, s$ ). The charm and bottom partons are turned on above scales ( $\mu_f = Q$ ) equal to the heavy quark masses,  $m_c = 1.3$  GeV and  $m_b = 4.5$  GeV. To be consistent with the most common applications of PDFs in collider phenomenology, once above the heavy quark mass thresholds, partons are treated as massless.

The input (non-perturbative) PDFs are defined at an initial scale  $\mu_f = Q_0 = 1.3$  GeV ( $= m_c$ ) using functional forms that meet certain criteria: (i) they must reflect *qualitative* physical behaviors expected at small  $x$  (Regge) and large  $x$  (quark counting rules); and (ii) they must be flexible enough to allow for unknown non-perturbative behavior (to be determined by fitting data)<sup>6</sup>; while (iii) they should not involve more free parameters than can be constrained by available data. In general, we use the functional form

$$xf(x, Q_o) = A_o x^{A_1} (1-x)^{A_2} e^{A_3 x} (1 + e^{A_4 x})^{A_5} \quad (1)$$

for each flavor (see [10] for motivation and explanation). This generic form is modified, as necessary to study specific issues (such as whether a negative gluon distribution at small  $x$  is indicated by data).

The experimental data sets that are used in the new analyses are essentially the same as those of CTEQ6, with minor updates.<sup>7</sup> As mentioned in the previous sections, the kinematic cuts on the input data sets are systematically varied as a part of the current stability study.

### 4 Results on the stability of NLO global analysis

The stability of our NLO global analysis is investigated by varying the inherent choices that must be made in performing the analysis. These choices include the selection of experimental

---

<sup>6</sup>Unnecessarily restrictive parametrized forms, which introduce artificial correlations between the behavior of PDFs in different regions of the  $x$  range, have been responsible for several wrong conclusions in past global QCD analyses.

<sup>7</sup>For instance, a third set of H1 data [13] has been added to the two sets used in [10].

data points based on certain kinematic cuts, the functional forms used to parametrize the initial non-perturbative parton distribution functions, and the treatment of  $\alpha_s$ . Section 4.1 concerns the kinematic cuts and the form of the gluon distribution, which relate directly to the “tension” found in [4] that motivated this study. Section 4.2 is about the choice of  $\alpha_s$ .

The stability of the results is most conveniently measured by differences in the global  $\chi^2$  for the relevant fits. To quantitatively define a change of  $\chi^2$  that characterizes a significant change in the quality of the PDF fit is a difficult issue in global QCD analysis. In the context of current global analysis, we have presented arguments that give an estimate of  $\Delta\chi^2 \sim 100$  (for  $\sim 2000$  data points) ([10, 14–16]) as roughly a 90% CL uncertainty on PDFs due to the uncertainties of the present input experimental data. This *tolerance* will provide a useful yardstick for judging the significance of the fits in our stability study, because currently available experimental data cannot distinguish much finer differences.<sup>8</sup>

## 4.1 Stability with respect to kinematic cuts on input data

The CTEQ6 and previous CTEQ global fits imposed “standard” cuts  $Q > 2$  GeV and  $W > 3.5$  GeV on the input data set, in order to suppress the possible effects of NNLO and power-law (“higher twist”) corrections. We examine in this section the effect of stronger cuts on  $Q$  to see if the fits are stable. We also examine the effect of imposing cuts on  $x$ , which should serve to suppress any effects due to deviations from DGLAP evolution, such as those of the type predicted by BFKL. The basic idea is that any inconsistency in the global fit due to data points near the boundary of the accepted region will be revealed by an improvement in the fit to the data that remain after those near-boundary points have been removed from the fit [4]. In other words, the decrease in  $\chi^2$  for the subset of data that is retained, when the shape parameters are refit to that subset alone, measures the degree to which the fit to that subset was distorted in the original fit by compromises imposed by the data at low  $x$  and/or low  $Q$ .

The main results of this study are presented in Table 1. Three fits are shown for the choices of the exclusionary cuts as specified in the table. They are labelled ‘standard, intermediate and strong.’  $N_{\text{pts}}$  is the number of data points that pass the cuts for each case;  $\chi^2_{N_{\text{pts}}}$  is the  $\chi^2$  value for that subset of data. The fact that the changes in  $\chi^2$  values in each column are insignificant compared to the uncertainty tolerance is strong evidence that our NLO global fit results are very stable with respect to choices of kinematic cuts. As an example, note that the subset of 1588 data points that pass the *strong* cuts ( $Q > 3.162$  GeV and  $x > 0.005$ ) are fit with  $\chi^2 = 1579$  when fitted alone; whereas the compromises that are needed to fit the full standard data set force  $\chi^2$  for this subset up to 1583. This small increase—only 4 in the total  $\chi^2$  for the large subset—is an order of magnitude smaller than what would represent a significant change in the quality of the fit according to our tolerance criterion for uncertainties.

---

<sup>8</sup>In the future, when systematic errors in key experiments are reduced and when different experimental data sets become more compatible with each other, this yardstick will also shrink in size.

Cuts	$Q_{\min}$	$x_{\min}$	$N_{\text{pts}}$	$\chi^2_{1926}$	$\chi^2_{1770}$	$\chi^2_{1588}$	$\sigma_W(LHC)$
standard	2 GeV	0	1926	2023	1850	1583	20.02
intermediate	2.5 GeV	0.001	1770	–	1850	1579	20.10
strong	3.162 GeV	0.005	1588	–	–	1579	19.98

Table 1: Comparisons of three fits for the choices of the exclusionary cuts on  $Q$  and  $x$  as indicated. In these fits, a conventional positive definite gluon parametrization is adopted.

We have extended the same analysis to a series of fits in which the gluon distribution  $g(x)$  is allowed to be negative at small  $x$  at the scale  $Q_0 = 1.3 \text{ GeV}$  where we begin the DGLAP evolution. The purpose of this additional study is to determine whether the feature of a negative gluon PDF is a key element of the stability puzzle, as suggested by the findings of [4]. The results are presented in Table 2. Even in this extended case, we find no evidence of instability. For example, for the subset of 1588 points that pass the *strong* cuts, the  $\chi^2$  for the subset increases only from 1571 to 1579 when the fit is extended to include the full standard data set. This result is very close to the corresponding positive gluon case.

Cuts	$Q_{\min}$	$x_{\min}$	$N_{\text{pts}}$	$\chi^2_{1926}$	$\chi^2_{1770}$	$\chi^2_{1588}$	$\sigma_W(LHC)$
standard	2 GeV	0	1926	2011	1845	1579	19.94
intermediate	2.5 GeV	0.001	1770	–	1841	1577	19.90
strong	3.162 GeV	0.005	1588	–	–	1571	20.63

Table 2: Same as Table 1 except the gluon parametrization is extended to allow for negative values.

Comparing the elements of Table 1 and Table 2 shows that our fits with  $g(x) < 0$  have slightly smaller values of  $\chi^2$ : e.g., 2011 versus 2023 for the standard cuts. However, the difference between these values ( $\Delta\chi^2 = 12$ ) is again not significant compared to our tolerance criterion.

Negative parton distributions in a given renormalization and factorization scheme are not strictly forbidden by theory. However, a PDF set that leads to any negative cross sections—either of practical importance or as a matter of principle—must be considered unphysical. Therefore to establish that a PDF set with negative PDFs is truly viable is very difficult: the negative PDFs can be enhanced in a special kinematic region for a specific cross section, leading to a negative cross section.<sup>9</sup>

Our results for a parametrization that allows  $g(x) < 0$  lead us to conclude that a negative  $g(x)$  may be permitted, but is certainly not indicated, by our analysis. Further discussion of this point, with specific examples from our fits and those of [4], is given in Appendix B.

<sup>9</sup>For instance, the negative gluon distributions of [4] do give rise to negative  $F_L$  (at low  $x$ ) and  $d\sigma_W/dy$  (at large  $|y|$  and high  $E$ ) [4].

Tables 1 and 2 also show the predicted cross section for  $W^+ + W^-$  production at the LHC. This prediction is also very stable: it varies only by  $< 0.5\%$ , ?? **The range in Table 1 appears to be  $\pm 0.8\%$ ; the range in Table 2 appears to be  $\pm 2.3\%$  ??** which must be compared to the PDF uncertainty of  $\sim 4\%$  on the prediction calculated by the 40 eigenvector uncertainty sets of CTEQ6.1. These results are explicitly displayed, and compared to the MRST results of Fig. 1, in Fig. 4. We see that this physical prediction is indeed insensitive

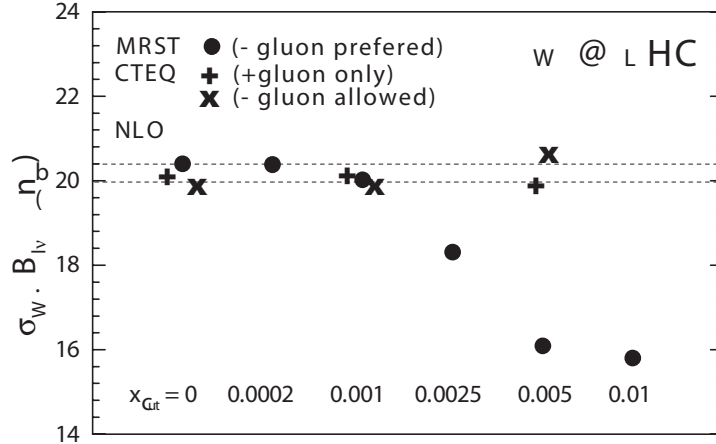


Figure 4: Predicted total cross section of  $W^+ + W^-$  production at the LHC for the fits obtained in our stability study, compared to the NLO results of Ref. [4] (cf. Fig. 1). The  $Q$ -cut values associated with the CTEQ points are given in the two tables. The overall PDF uncertainty of the prediction is  $\sim 4\%$ .

to the kinematic cuts used for the fits, and to the assumption on the positive definiteness of the gluon distribution. A more focused study on the uncertainty of this prediction and its variation with the kinematic cuts, using the Lagrange Multiplier method, is given in Sec. 5.

The stability of the NLO global fits with respect to cuts on  $x$  and  $Q$  demonstrated in this section is consistent with the expected numerical accuracy of the PQCD expansion, and is in apparent disagreement with the findings of [4]. The two analyses differ in several ways. One difference concerns the treatment of  $\alpha_s$ , which we examine next.

## 4.2 Stability and $\alpha_s$

The CTEQ5/6/6.1 PDF sets were extracted assuming  $\alpha_s(m_Z) = 0.118$ . This value was chosen to approximate the World Average, thereby to incorporate the rather strong constraints from data—especially those from LEP—that are not otherwise included in our global data set. To examine the influence of  $\alpha_s(m_Z)$  on the quality and stability of the fit, we have made a series of fits with different choices for  $\alpha_s(m_Z)$ . This exercise provides a further test of the reliability of the fit.

Our results for  $\chi^2$  as a function of  $\alpha_s(m_Z)$  take the parabolic form shown as the solid curve in the left hand side of Fig. 5. Qualitatively, the value of  $\alpha_s(m_Z)$  preferred by the

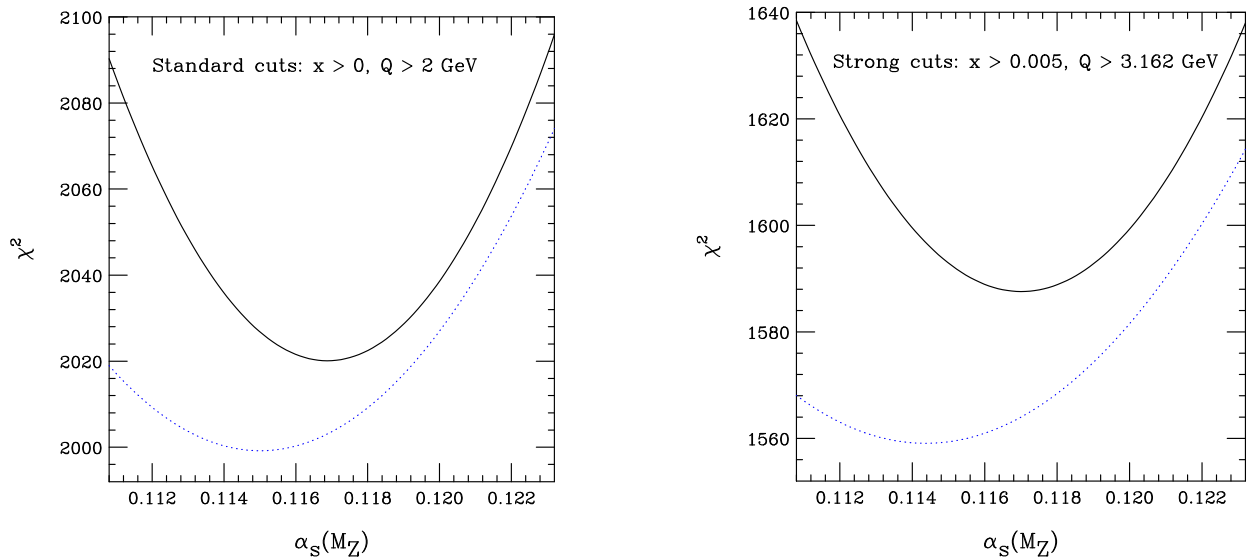


Figure 5: The global fit  $\chi^2$  as a function of  $\alpha_s(m_Z)$  with *Standard* data cuts. Solid curve assumes  $g(x) > 0$ ; Dotted curve allows  $g(x) < 0$ .

global fit is in reasonable agreement with the World Average, which lends support to the idea that NLO QCD is working successfully in the global fit. To obtain a quantitative result, we take  $\Delta\chi^2 = 25$  to define a  $1\sigma$  error (based on a 90% C.L. range of  $\Delta\chi^2 = 100$  as previously mentioned). In this way we obtain

$$\alpha_s(m_Z) = 0.1169 \pm 0.0036 \quad (2)$$

from the PDF fit using the standard data cuts. This shows good consistency with the current world average  $0.1187 \pm 0.0020$ [17], and with the LEP QCD working group average  $0.1201 \pm 0.0003 \pm 0.0048$ . The consistency lends confidence to the standard analysis—including the “standard” data cuts used in it. The average  $\chi^2$  per data point at the minimum is  $\chi^2/N = 2020/1926 = 1.049$ , which is comfortably close to 1.

The solid curve in the right hand figure of Fig. 5 shows the effect of imposing the “strong” data cuts ( $Q > 3.162 \text{ GeV}$ ,  $x > 0.005$ ). The allowed range in  $\chi^2$  should scale as the number of data points, so we can estimate the  $1\sigma$  uncertainty range in the case of the strong cuts as the range over which  $\chi^2$  increases by  $25 \times (1588/1926)$  above its minimum value. This leads to  $\alpha_s(m_Z) = 0.1170 \pm 0.0040$ . With the additional cuts, the location of the minimum shifts by only a tiny amount compared to its error. This shows that the fit is very stable with respect to the cut. The uncertainty in  $\alpha_s(m_Z)$  increases slightly when the strong cuts are imposed, as would be expected since less data is being used.

The dotted curves in Fig. 5 show the effect of allowing the gluon distribution  $g(x)$  to be negative at small  $x$  and small  $Q$ . This modification causes little change in the fitting for  $\alpha_s(m_Z)$ ; this point is discussed further in Appendix A.

In addition to the possible range of values of  $\alpha_s(m_Z)$ , there is an uncertainty caused by

ambiguity in how to define  $\alpha_s(Q)$  at NLO. We show in Appendix A that this ambiguity has little effect on the results of the global fits or their stability.

### 4.3 Comments and Discussions

The remarkable stability of the global fits shown by the results for  $\chi^2_{1770}, \chi^2_{1588}, \chi^2_{638}$  in Tables 1 and 2, and by the results for  $\sigma_W^{\text{LHC}}$  shown in those Tables and in Fig. 4, is reassuring. It confirms the general expectations of the PQCD expansion. It lends confidence to the extensive NLO QCD phenomenological work that is being done in connection with current and future collider physics programs. However, we must still ask why our results differ from those of [4]. Two separate issues are involved in the comparison between the two global analysis programs.

First, the instability of the NLO analysis observed in [4] appeared originally result from a “tension” between the Tevatron inclusive jet data (mostly at medium and large  $x$ ) and the DIS data at small  $x$  (HERA) and medium  $x$  (NMC). This tension has been a consistent feature in all recent MRST analyses. However, CTEQ analyses, including the current study, have consistently not seen this tension. The difference is most likely due to the behavior of the gluon distribution function at large  $x$ . The CTEQ input gluon distribution is consistently higher in the large  $x$  region, which allows a much better fit to the CDF and D0 jet production cross section, without affecting the fits to the DIS data. This point has been confirmed recently by a new MRST paper [12] that uses an input gluon distribution quite similar in shape to the CTEQ  $g(x)$ . We compare the large- $x$  behavior of the relevant PDF sets in Appendix C.

The second issue concerns negative gluons at small  $x$ .<sup>10</sup> Whereas we find only marginal differences in the quality of the global fits when the input gluon function is allowed to become negative, MRST has found a strong pull toward negative gluon in their analyses. Furthermore, the gluon distribution becomes increasingly negative as the  $x$  cut is raised. The increasingly negative gluon distribution at small  $x$ , together with its influence on the sea quark distributions due to QCD evolution, is directly responsible for the rapid decrease of  $d\sigma_W^{\text{LHC}}/dy$  outside the central rapidity region, and consequently the decrease of the total  $\sigma_W^{\text{LHC}}$ , as seen in Fig. 1. Further details on the behavior of the relevant PDFs at small  $x$  are described in Appendix B.

The source of the different conclusions about a negative gluon PDF has not been (**conclusively/convincingly/definitively/...**) identified. But because the improvement to the fit is small, and because of the reservations expressed earlier about negative PDFs in general, we do not believe that allowing negative gluons is necessary to the global analysis.

---

<sup>10</sup>Although initially thought to be related to the large- $x$  issue through momentum sum rule constraints, the connection is less clear now, because of the advance in [12].

## 5 Stability and Uncertainty of $\sigma_W^{\text{tot}}$ at the LHC

In this section, we study in detail the stability of the NLO predictions for the cross section  $\sigma_W^{\text{tot}}$  for  $W^+ + W^-$  production at the LHC, using the robust Lagrange Multiplier (LM) method of Refs. [14–16].  $W$  production will be a standard-candle process at the LHC, so the theoretical uncertainty of its prediction is important. In this study we perform a series of dedicated fits to the global data constrained to specific values of  $\sigma_W^{\text{tot}}$  around that predicted by the best fit. The variation of  $\chi^2$  versus  $\sigma_W^{\text{tot}}$  measures the uncertainty of the prediction. We repeat the constrained fits for each case of fitting choices (parametrization and kinematic cuts). In this way we obtain a fuller understanding of the stability than can be obtained by looking only at the central predictions.

The results for each series are expressed as the curve of  $\chi^2$  as a function of  $\sigma_W^{\text{LHC}}$ . The LM method fully explores the parton distribution parameter space. It allows us to map out the range of uncertainty of  $\sigma_W^{\text{tot}}$  for each of the cases investigated.

Figure 6 shows the results of the Lagrange Multiplier (LM) study for the four sets of kinematic cuts described in Table 1, all of which have a positive definite gluon distribution. The  $\chi^2$  shown along the vertical axis is normalized to its value for the best fit in each

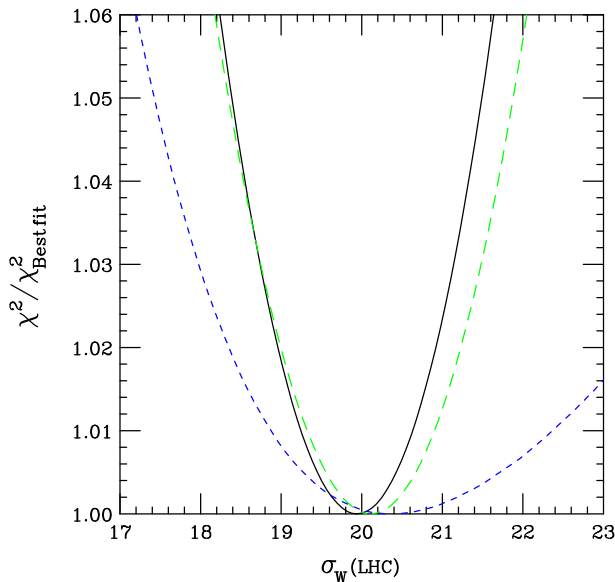


Figure 6: Lagrange Multiplier results for the  $W$  cross section at the LHC using a positive-definite gluon. The three curves, in order of steepness, correspond to the three sets of kinematic cuts labelled standard/intermediate/strong in Table 1.

series. Neither the absolute value of  $\chi^2$ , nor its increment above the respective minimum, are suitable for comparison, because the different cuts render the number of data points quite different for the four cases. Instead we look at the ratios to the best fit for each series. In all four series,  $\chi^2$  depends almost quadratically on  $\sigma_W^{\text{tot}}$ . We observe several features:

- The location of the minimum of each curve represents the best-fit prediction for  $\sigma_W^{\text{LHC}}$  for the corresponding choice of exclusionary cuts. The fact that the four minima are close together displays the stability of the predicted cross section (cf. Table 1).
- Although more restrictive cuts make the global fit less sensitive to possible contributions from resummation, power-law and other nonperturbative effects, the loss of constraints due to the removal of precision HERA data points at small  $x$  and low  $Q$  results directly in increased uncertainties on the PDF parameters and their physical predictions. This is shown in Fig. 6 by the increase of the width of the curves with stronger cuts. The uncertainty of the predicted  $\sigma_W^{\text{tot}}$  doubles from the standard cuts to the strong cuts.

The left-side plot in Fig. ?? shows the results for the standard/intermediate/strong cut cases summarized in Table 2 when the gluon distribution is allowed to be negative at small  $Q$  and  $x$ . In this case, we observe:

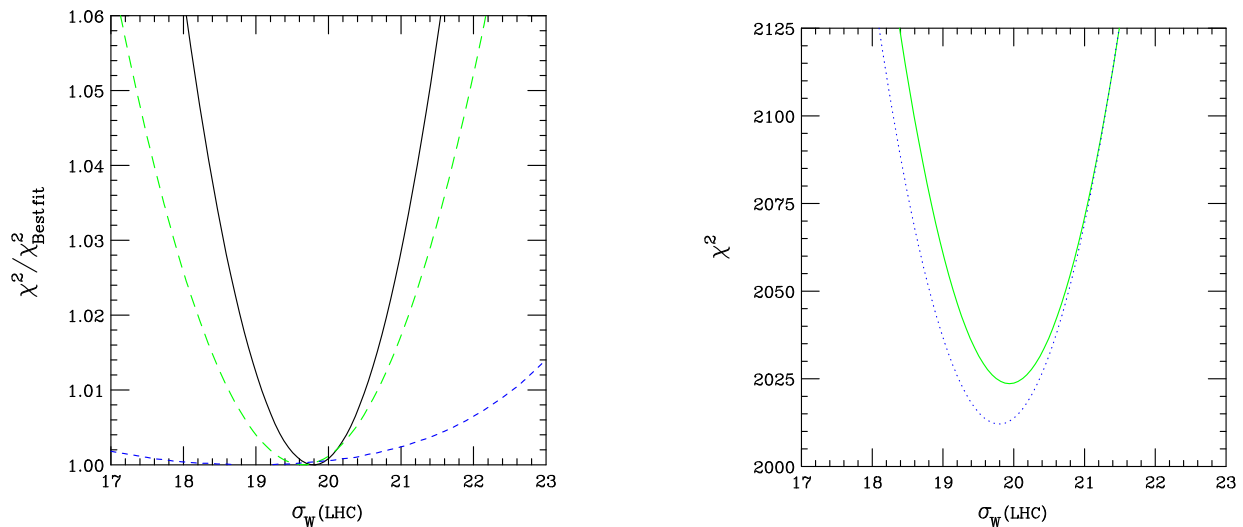


Figure 7: Left plot: The LM results for the  $W$  cross section at the LHC allowing negative gluon PDF. The three curves, in order of steepness, correspond to the sets of kinematic cuts labelled standard/intermediate/strong in Table 2. Right plot: Comparison of the two cases of standard cuts, i.e., with or without restricting the gluon to be positive definite. The negative gluon fit is slightly lower at the minimum, but the difference is not significant.

- The stability of the best fits, represented by the minima of the curves, is again apparent. In other words, there is no advantage of imposing the stronger cuts.
- With strong cuts and allowing negative gluons, the uncertainty range of  $\sigma_W^{\text{tot}}$  expands considerably, especially toward low values of  $\sigma_W^{\text{tot}}$ . The solutions at the extreme low end of the  $\sigma_W^{\text{tot}}$  range are most likely unphysical. The negative gluon distribution at small  $x$  and  $Q$  can drive the quark distributions negative at  $x \sim 10^{-4}$  and moderate values of  $Q$  by QCD evolution, cf. Appendix B.

The right-side plot of Fig. ?? shows the comparison of the two LM series both using the standard cuts, but with or without the positive definiteness requirement. We observe:

- Removing the positive definiteness condition necessarily lowers the value of  $\chi^2$  (because more possibilities are opened up in the  $\chi^2$  minimization procedure), but the decrease is insignificant compared to other sources of uncertainty. Thus, a negative gluon PDF is allowed, but not required.
- The minima of the two curves occur at approximately the same  $\sigma_W^{\text{tot}}$ . Allowing a negative gluon makes no significant change in the central prediction, but merely a decrease of about 1%. This difference is small compared to the overall PDF uncertainty from experimental error, which is  $\sim 4\%$ .
- For the standard set of exclusionary cuts, allowing a negative gluon PDF expands the uncertainty range. For instance, using the  $\Delta\chi^2 = 100$  criterion, the range of the prediction increases from  $18.5 < \sigma_W^{\text{tot}} < 21.5$  to  $18.2 < \sigma_W^{\text{tot}} < 21.5$ .

## 6 Conclusions

Motivated by its importance to all aspects of collider physics phenomenology at the Tevatron and the LHC, we have examined the stability of the NLO QCD global analysis with respect to certain variations in its input, in particular, the selection of input experimental data and the functional form of the nonperturbative gluon distribution.

As increasingly stringent kinematic cuts at lower  $x$  and  $Q^2$  are placed on the input data (in order to exclude potentially theoretically unsafe regions of phase space), we found no significant improvement in the quality of the fit, as measured by the global  $\chi^2$  of the data kept. In particular, we do not observe the ‘tension’ discussed in recent MRST analyses. Simultaneous good fits of the HERA and Tevatron jet data are obtained for the full range of cuts explored. Predictions for the W cross section at both the Tevatron and LHC were examined. As data at lower  $x$  and  $Q^2$  are removed from the analysis, the central value remains quite stable, but the uncertainty on the predicted total W cross section increases. This has important implications, for example, on the use of the W cross section as a benchmark process for the Tevatron and the LHC.

We have also performed the same analyses allowing the gluon distribution to assume negative values in some regions of phase space, a possibility strongly favored by the MRST study. There is a slight reduction in the global  $\chi^2$  (which is expected when the fitting parameter space is expanded), but the size of the reduction is well within the uncertainty of the analysis, hence is of no physical significance in our analysis framework. The predicted  $W^\pm$  cross sections remain very stable under this variation, as for the case of kinematic cuts. The uncertainties on the cross sections again increase somewhat, as expected.

In summary, we have found the NLO PDFs and their physical predictions at the Tevatron and LHC to be quite stable with respect to variations of the kinematic cuts and the

PDF parametrization. Thus, the NLO framework should provide sufficient accuracy for phenomenology at both Run II at the Tevatron and at the LHC. Further improvement will be possible with a NNLO global QCD analysis framework, but the size of the improvement is expected to be relatively small; in addition, a truly global analysis must wait for the completion of the calculation of the inclusive jet cross section at NNLO.

**Acknowledgement:** We would like to thank Robert Thorne for many informative and stimulating communications concerning the similarities and differences of the the MRST and CTEQ analyses.

## A Treatment of $\alpha_s(Q)$

A subtle difference between various NLO global analyses arises from the choice of definition for the variation of  $\alpha_s(Q)$  at NLO. The various choices differ only at NNLO, so they are equally valid, *a priori*, at NLO. The principal definitions in use are

1. Exact solution of the truncated renormalization group equation:

$$\mu d\alpha/d\mu = c_1\alpha^2 + c_2\alpha^3, \quad (3)$$

where  $c_1 = -\beta_0/2\pi$  with  $\beta_0 = 11 - (2/3)n_f$ , and  $c_2 = -\beta_1/8\pi^2$  with  $\beta_1 = 102 - (38/3)n_f$ . This is the recipe used in the QCD evolution program QCDNUM [18], which is used by several groups, including ZEUS.

2. The original  $\overline{\text{MS}}$  definition at NLO [19]:

$$\alpha(Q) = c_3 [1 - c_4 \ln(L)/L]/L, \quad (4)$$

where  $L = \ln(Q^2/\Lambda^2)$ ,  $c_3 = -2/c_1$ , and  $c_4 = -2c_2/c_1^2$ . This is the definition used in CTEQ global analyses.

3. The form chosen by MRST is less simple to state: for  $Q > m_b$  it contains a NNLO term that depends on  $1/\alpha(m_b) - 1/\alpha(m_c)$ . However, it is numerically very similar to the QCDNUM choice.

Fig. 8 shows that MRST and QCDNUM forms are very similar; and that the difference between them and the CTEQ form is quite small in the region  $Q > 2 \text{ GeV}$  where we fit data. In particular, that difference is much smaller than the difference caused by changing  $\alpha_s(M_z)$ .

The dependence of  $\chi^2$  for the global fit on  $\alpha_s(m_Z)$  is shown in Fig. 9 for *standard* and *strong* cuts. One sees that the choice of form for  $\alpha_s(Q)$  has very little effect on the quality of the global fit, which is a satisfying indication of the stability of the fit with respect to one of the arbitrary choices that is necessary to carry it out. The similarity of the two figures shows that the fit is stable with respect to kinematic cuts as well.

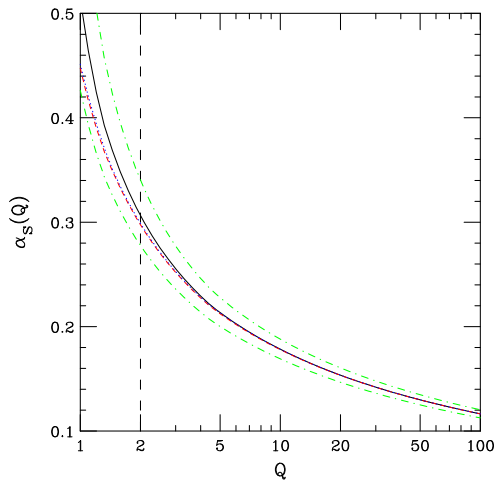


Figure 8: The dependence of  $\alpha_s(Q)$  on  $Q$ . Solid curve is CTEQ form with  $\alpha_s(m_Z) = 0.118$ ; Dashed curve is QCDNUM form with  $\alpha_s(m_Z) = 0.118$ ; Dotted curve is MRST form with  $\alpha_s(m_Z) = 0.118$ . Dot-dash curves are CTEQ form with  $\alpha_s(m_Z) = 0.114, 0.122$ .

In detail, the two choices produce slightly different best-fit values for  $\alpha_s(m_Z)$ . This can easily be understood using Fig. 8: for a given  $\alpha_s(m_Z)$ , the QCDNUM choice gives a slightly smaller  $\alpha_s(Q)$  in the region of  $Q$ —mostly much smaller than  $m_Z$ —that is important in the fit.

The uncertainties of  $\alpha_s(Q)$  lead to an uncertainty in the prediction for  $\sigma_W$  at the LHC. In particular, the four fits with standard cuts, which are shown in Fig. 9a, span a range of  $\pm 1.5\%$  ( $\pm 2.8\%$ ) in  $\sigma_W$  for  $\alpha_s(m_Z) = 0.116 - 0.120$  ( $0.114 - 0.122$ ). The four fits with *strong* cuts, shown in Fig. 9b, span a much larger range:  $\pm 5.8\%$  ( $\pm 9.2\%$ ) in  $\sigma_W$ . Once again, we see the loss of predictive power of NLO QCD analysis when too much data is removed from the input.

## B PDFs at small $x$ : do they go negative?

As mentioned in the text, the behavior of the gluon distribution (and through DGLAP evolution, the sea quark distributions) at small  $x$  and low  $Q$  appears to be an open issue at the present time. In particular, there is a question of whether the data allow or suggest that these distributions become negative at small  $x$ . We discuss the situation in more detail in this section.

Fig. 9 shows that allowing  $g(x) < 0$  (by inserting a factor  $(1 + ax^b)$  into the standard CTEQ parametrization for  $g(x)$  at  $Q_0 = 1.3$  GeV, with  $a$  and  $b$  allowed to be negative) leads to a small improvement in the global fit:  $\chi^2$  decreases by about 20 (the difference between the minima of the top two and bottom two curves). This decrease is again well within the tolerance of our uncertainty range—especially in view of the fact that almost *any* additional freedom in the fitting functions can be expected to produce at least a small decrease in

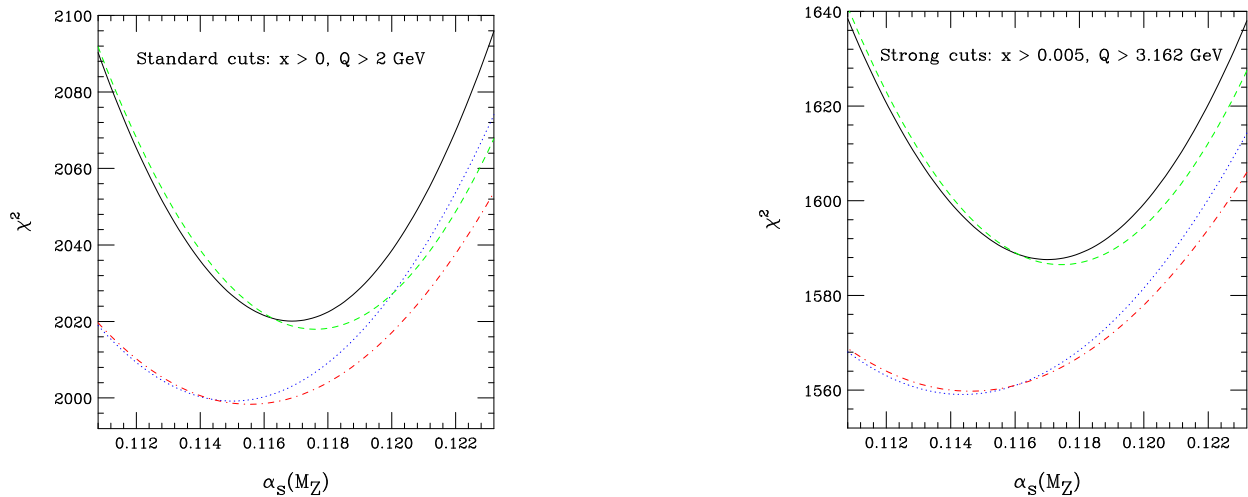


Figure 9: The global fit  $\chi^2$  as a function of  $\alpha_s(m_Z)$  for *Standard* cuts (left) and *strong* cuts (right). Solid curve uses CTEQ form for  $\alpha_s(Q)$ ; Dashed curve uses QCDNUM form for it. These curves assume positive gluons; the corresponding curves if  $g(x) < 0$  is allowed are Dotted (CTEQ) and Dot-dash (QCDNUM).

$\chi^2$ . The change in  $\chi^2$  is a little larger in the case of the *strong* data cuts (Fig. ??)—about 28—but still not persuasive.

The MRST2003c NLO fit has a much more negative gluon than any of the fits described here. Its negative region is so strong that it evolves to produce negative sea quark distributions for  $x < 2 \times 10^{-5}$  (see figure in appendix) at  $Q = 100$  GeV. The suppression of these sea quark distributions at small  $x$  near where they pass through zero is responsible for the much smaller  $\sigma_W$  (16.12) predicted for LHC by MRST2003cnlo. We are able to reproduce this suppression in our fits that allow a negative  $g(x)$  at  $Q_0$  only by simultaneously (1) imposing the *strong* data cuts on  $x$  and  $Q$ ; and (2) increasing the fit  $\chi^2$  by  $\sim 20$  units by employing the Lagrange Multiplier method to force  $\sigma_W$  downward. Although this modest increase in  $\chi^2$  is acceptable according to our tolerance criteria, the stability of our fits with respect to the cuts renders it unnatural to impose the strong cuts. Furthermore, negative sea quark distributions at  $Q$  as large as  $Q = 100$  GeV are at best unattractive. For example, the MRST2003c NLO PDFs predict their suppressed  $W$  cross section in pp scattering at  $\sqrt{s} = 14$  TeV because  $W$ 's are produced at large rapidity by annihilation of a quark at large  $x$  with an antiquark at very small  $x$ ; at a slightly higher energy, say  $\sqrt{s} = 40$  TeV, the same PDFs predict a substantial region of negative cross section at large rapidity. But one would not expect such a dramatic failure of the NLO prediction at such a large value of  $Q$ .

Figure 10 shows the  $\bar{u}(x)$  distribution at  $Q = 100$  GeV. ( $u(x)$ ,  $d(x)$ ,  $\bar{u}(x)$ ,  $\bar{d}(x)$  are nearly identical at small  $x$ .) The CTEQ6.1 (solid) and MRST2002 (long dash) curves are very similar, while MRST2003c (short dash) turns negative at small  $x$ . Our best fit with  $g(x) < 0$  (dotted) is quite similar to CTEQ6.1. Even when  $\sigma_W$  is forced smaller by a

Lagrange multiplier that raises  $\chi^2$  by 70, the distribution is not greatly different (dot-dash). Substantially different behavior is obtained only we impose the *strong* data cuts and force  $\sigma_W$  small by a Lagrange multiplier (dot-dot-dash).

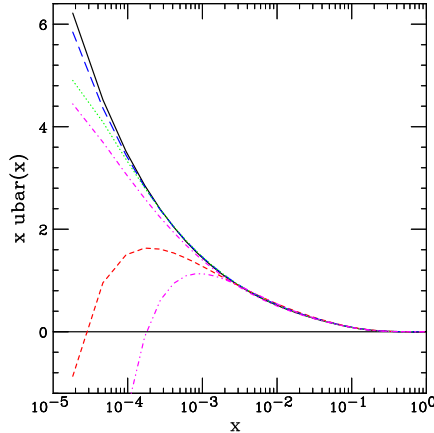


Figure 10:  $x \bar{u}(x)$  distributions at  $Q = 100$  GeV. Solid=CTEQ6.1, long dash=MRST2002, short dash=MRST2003c. Dotted= $g(x) < 0$ ; dot-dash= $g(x) < 0$  with  $\sigma_W$  pushed low by Lagrange Multiplier; dot-dot-dash= $g(x) < 0$  with  $\sigma_W$  pushed low by Lagrange Multiplier using *strong* cuts.

## C Gluon distribution at large $x$ : do counting rules count?

The behavior of the gluon distribution at large  $x$  strongly affect how well one can fit the inclusive jet production data. This has a direct bearing on whether the jet data can be described simultaneously with the precision DIS data, in the NLO global analysis framework, as discussed in the text.

Fig. 11a shows the gluon distributions at  $Q = 100$  GeV for various PDF fits. The solutions that fit the jet data best are those with a rather strong gluon at large  $x$ . The solid curve is CTEQ6.1. The two dotted curves are eigenvector sets 29 and 30, which are the members of the 40 eigenvector uncertainty PDF sets that have the most extreme gluon distributions. MRST2002 lies just at the edge of this range of uncertainty, which presumably accounts for the “tension” MRST find between DIS and Jets with this solution. MRST2003c is slightly closer to the CTEQ result, while MRST2004 is much closer to it.

In all PDF analyses, the gluon distribution at  $Q_0$  has been parametrized in a form that varies as  $(1-x)^a$  as  $x \rightarrow 1$ . We have treated  $a$  as a free parameter in the fitting, just like all of the other parton shape parameters at  $Q = 1.3$  GeV. Fig. 11b shows the gluon distributions as a function of  $1-x$  on a Log-Log plot. The approximately straight-line behavior at small  $1-x$  shows that an effective  $(1-x)^a$  dependence survives the inclusion of effects due to

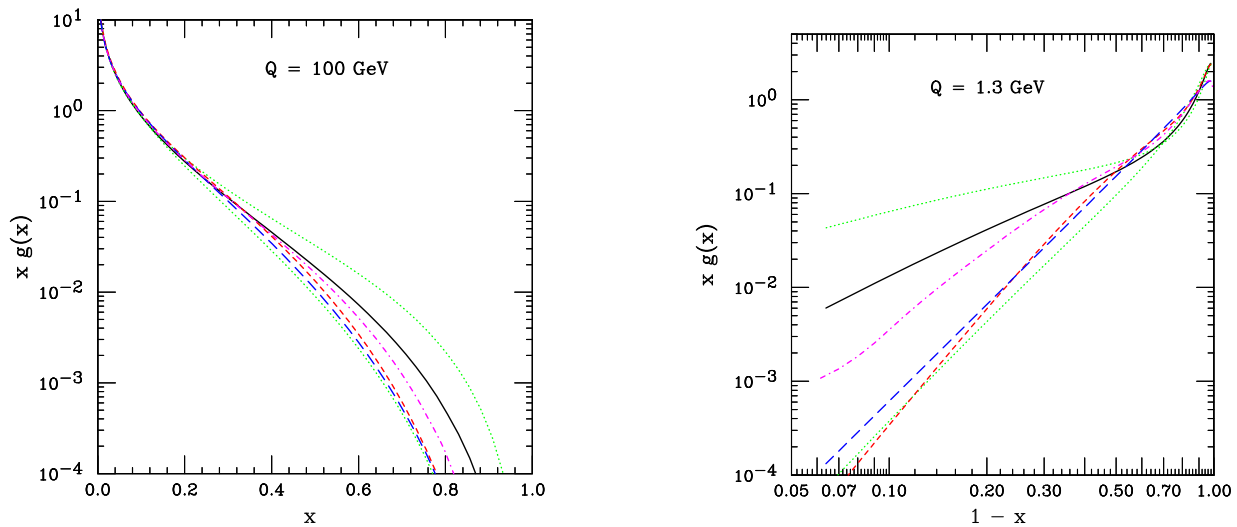


Figure 11: Gluon at  $Q = 100$  GeV, (a); and  $Q = 1.3$  GeV, (b). Solid curve is CTEQ6.1; long dash is MRST2002; short dash is MRST2003c; dot-dash is MRST2004. Dotted curves are extreme gluon distributions (sets 29 and 30) from the 40 uncertainty eigenvector sets.

other parameters. From the slope of the straight lines, we find that the effective power  $a$  is about 1.7 for CTEQ6.1, and varies from 0.8 to 3.6 over the 40 eigenvector sets.

MRST2003c has  $a \approx 3.5$ , similar to the steepest fall-off of the 40 uncertainty sets of CTEQ6.1. MRST2002 is even steeper at  $a \approx 4.1$ . This difference between the MRST and CTEQ fits may be because of an attempt to satisfy the “counting rules,” [20] which would predict a much faster fall-off for gluons than for valence quarks at  $x \rightarrow 1$ .

Whatever one may think of the underlying basis for the counting rules, recent work by MRST has shown that the effect of assuming them is highly dependent on the QCD Scheme—e.g., assuming the relation in the DIS representation is very different from assuming it in  $\overline{\text{MS}}$ , as MRST have shown recently. Hence the CTEQ procedure of ignoring the rule is the best course.

It is quite re-assuring that the  $(1-x)^a$  behavior of the *valence quark* distributions determined by the global fit are actually in rather good agreement with expectations from quark counting rules.)

## References

- [1] AlekhinNnlo
- [2] Mrstnlo
- [3] NnloKernel
- [4] mrst03

- [5] alekhin
- [6] zeus
- [7] h1
- [8] gkk
- [9] cteqjet
- [10] cteq6
- [11] Eur. Phys. J. C **28**, 455 (2003).
- [12] mrst04
- [13] H1new
- [14] MultiVar
- [15] LM
- [16] Hesse
- [17] PDG
- [18] QcdNum
- [19] MsbAlf
- [20] counting rules